JOURNAL OF CATALYSIS **164,** 207–219 (1996)
ARTICLE NO. 0376

FTIR and ^{31}P-NMR Spectroscopic Analyses of Surface Species in Phosphate-Catalyzed Lactic Acid Conversion

Garry C. Gunter,* Radu Craciun,† Man S. Tam,* James E. Jackson,† and Dennis J. Miller*,[1]

*Department of Chemical Engineering and †Department of Chemistry, Michigan State University, East Lansing, Michigan 48824

Received February 15, 1996; revised June 12, 1996; accepted July 15, 1996

The surface species present on silica/alumina-supported sodium phosphates, active catalysts for the conversion of lactic acid to acrylic acid and 2,3-pentanedione, are examined by pre- and postreaction MAS ^{31}P-NMR and FTIR spectroscopies. Species present following lactic acid conversion are identified by transmission FTIR of phosphates supported on silicon disks (as a model catalyst system) and verified by ^{31}P-NMR and diffuse reflectance IR spectroscopy of actual catalysts used in reaction. Monosodium phosphate (NaH_2PO_4) condenses to a mixture of sodium polyphosphate $(NaPO_3)_n$ and sodium trimetaphosphate ($Na_3P_3O_9$), which exhibit little catalytic activity for converting lactic acid to desired products. Disodium phosphate (Na_2HPO_4) condenses to tetrasodium pyrophosphate ($Na_4P_2O_7$), and proton transfer from lactic acid to pyrophosphate results in the formation of sodium lactate. Trisodium phosphate (Na_3PO_4) accepts a proton from lactic acid to form sodium lactate and disodium phosphate, which condenses to pyrophosphate. The presence of pyrophosphate and sodium lactate on supported disodium and trisodium phosphates explains their similar catalytic properties; the larger quantity of sodium lactate present on trisodium phosphate leads to higher conversions at lower temperatures.

I. INTRODUCTION

Lactic acid (2-hydroxypropanoic acid) is gaining importance as a potential chemical feedstock as new technologies for its manufacture reach commercialization. These highly efficient fermentation technologies, based on agriculturally derived starches, make available plentiful, low-cost lactic acid and its derivatives.

A variety of specialty and commodity chemicals can be produced from the catalytic conversion of lactic acid; conversion pathways pertinent to this work are given in Fig. 1. Most studies in the literature have focused on the conversion of lactic acid to acrylic (propenoic) acid in either vapor-phase (1–3) or supercritical water environments (4, 5). Acrylic acid yields as high as 68% have been reported (3), but the conversion is complicated by acetaldehyde-forming processes that compete with the desired pathway.

We have studied lactic acid conversion in our laboratories using simple phosphates (6) and other salts (7) as catalysts on well-defined supports. These studies led to the discovery of 2,3-pentanedione formation from lactic acid at mildly elevated pressures (0.5 MPa) and temperatures of 280–350°C. We have found that yield of 2,3-pentanedione is enhanced with increasing basicity of the salt catalyst, and that low-surface-area supports are preferred to avoid lactic acid carbonization and catalyst fouling. Representative results of prior lactic acid conversion studies (6) over the phosphate catalysts investigated in this paper are given in Table 1. A thorough evaluation of these conversion results, including presentation of a kinetic model of the reaction system, is given in the earlier work (6). Two important points warrant highlighting. First, acrylic acid and 2,3-pentanedione are only formed in meaningful quantities over disodium and trisodium phosphates; product selectivities are similar over these two salts, with the trisodium salt giving higher product yields at low temperature. Second, the support alone has almost no activity for acrylic acid and 2,3-pentanedione formation. Lewis and Brønsted acid sites on the Si/Al support, identified by pyridine adsorption (7), result in lactic acid decarbonylation to form acetaldehyde and coking of the support as dominant reaction pathways. Addition of basic sodium phosphate salts neutralizes these sites and reduces the extent of these undesirable reactions.

This paper describes the first study aimed at elucidating the mechanism of 2,3-pentanedione formation from lactic acid. The goal here is to identify stable species present on the surface of phosphate catalysts following lactic acid conversion, and to relate the presence of these species to trends in product selectivity and yield in phosphate-catalyzed conversion studies such as those described in Table 1. Thermal transformations of supported sodium phosphates are analyzed via magic angle spinning (MAS) ^{31}P-NMR spectroscopy to identify the form of the catalyst at reaction temperatures, and stable species on the catalyst surface are identified via postreaction Fourier transform infrared (FTIR) and ^{31}P-NMR spectroscopies.

[1] To whom correspondence should be addressed. E-mail: millerd@che.msu.edu.

0021-9517/96 $18.00

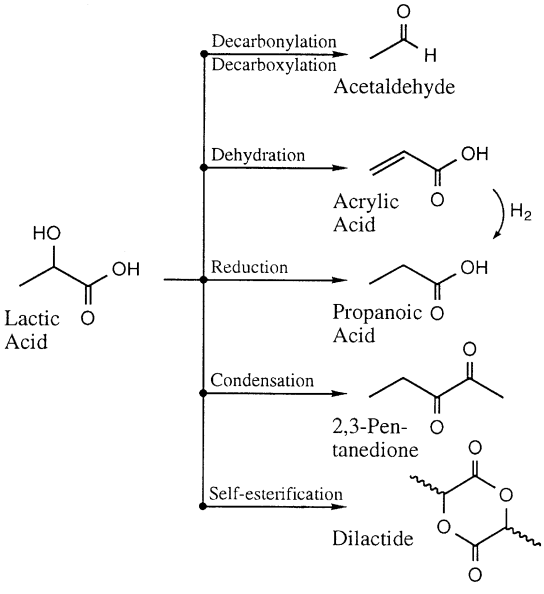

FIG. 1. Catalytic conversion pathways of lactic acid.

II. BACKGROUND

II.1. Thermal Transformations of Phosphates

Phosphate salts exist in a number of forms depending on temperature and extent of substitution. The orthophosphate salts of sodium, for example, can exist in monobasic, dibasic, and tribasic forms. Upon heating, monosodium and disodium phosphates condense to form chains and rings of various sizes (8). Partial dehydration of monosodium phosphate gives disodium pyrophosphate ($Na_2H_2P_2O_7$). Further heating above 220°C results in the formation of, depending on conditions, Maddrell's salt $(NaPO_3)_n$, a linear polyphosphate usually exhibiting some crosslinking, or trimetaphosphate ($Na_3P_3O_9$), a trimeric ring structure, in increasing amounts as heating continues up to the melting point of 625°C. These salts exist in several crystalline forms and degrees of hydration which can be prepared at different conditions. Other forms of salts exist in the system Na_2O–P_2O_5–H_2O, but most of them are not very stable (8, 9).

Heating disodium phosphate results in dehydration to tetrasodium pyrophosphate ($Na_4P_2O_7$) around 250°C; the pyrophosphate is stable to temperatures above 800°C. Trisodium phosphate is stable to temperatures above 900°C (9).

II.2. NMR of Phosphates

Magic angle spinning ^{31}P nuclear magnetic resonance (MAS ^{31}P-NMR) spectroscopy has been widely used to characterize phosphate salts (10–14). Chemical shifts of the various phosphates fall into distinct regions: orthophosphates exhibit the highest chemical shift, metaphosphates the lowest, and pyrophosphates have intermediate shifts. Several studies (10, 13, 14) have correlated factors that determine the ^{31}P chemical shifts in phosphates. These include the number and electronegativities of ligands on phosphorus, the bond angles about phosphorus, the occupation of π-bonding orbitals of phosphorus, and the effective nuclear charge and radius of the cation. As an example, the observed difference in chemical shift between terminal and central phosphorus in pentasodium triphosphate ($Na_5P_3O_{10}$) is attributed to increased π-bonding to terminal phosphorus atoms (10).

For each NMR signal, magic angle spinning produces an isotropic peak accompanied by spinning sidebands of varying intensities spaced at integer multiples of the spinning frequency on each side of the isotropic peak. The

TABLE 1

Product Yields[a] (Selectivities[b]) from Lactic Acid[c] over Phosphate Salts on Silica/Alumina Support (6)

	300°C				350°C			
Product	Support only	NaH_2PO_4	Na_2HPO_4	Na_3PO_4	Support only	NaH_2PO_4	Na_2HPO_4	Na_3PO_4
Acrylic acid	0.1 (1)	0.1 (6)	0.6 (17)	2.0 (14)	0.8 (4)	1.5 (17)	9.7 (29)	9.8 (31)
2,3-Pentanedione	0.2 (3)	0.2 (11)	1.6 (44)	4.3 (31)	0.3 (2)	1.3 (15)	8.1 (24)	7.0 (22)
Acetaldehyde	1.5 (22)	0.4 (22)	0.7 (19)	1.9 (14)	9.0 (48)	2.5 (28)	6.2 (19)	5.2 (16)
Propanoic acid	0.5 (7)	0.1 (6)	0.2 (6)	0.9 (6)	1.2 (6)	1.7 (20)	2.7 (8)	1.5 (5)
Hydroxyacetone	0.1 (1)	0.1 (6)	0.1 (3)	0.6 (4)	0.4 (2)	0.4 (5)	3.3 (10)	2.9 (9)
Other	4.3 (60)	0.9 (50)	0.4 (11)	4.2 (30)	7.2 (38)	1.3 (15)	3.4 (10)	5.2 (16)
CO	1.1	0.4	0.3	0.6	10.6	1.6	2.1	3.0
CO_2	0.2	0.2	0.9	5.0	1.9	2.1	9.7	10.2
Lactic acid conversion	6.5	1.8	3.4	14.1	18.6	8.7	33.4	32.6
Carbon recovery (%)	100.8	104.3	97.8	94.2	101.2	91.1	87.9	92.7

[a] Percent of theoretical yield for condensible products; CO and CO_2 yields are moles per 100 moles lactic acid fed to reactor.
[b] Percent of converted lactic acid which goes to each product.
[c] Feed is 0.5 ml/min of 34 wt% lactic acid in water plus 100 ml/min He, vaporized prior to contacting catalyst; total pressure is 0.5 MPa, residence time 0.3 s.

asymmetry of these spinning sidebands for many phosphates provides additional information about the environment of the associated phosphorus atoms (15–17).

II.3. Infrared Spectroscopy

Infrared spectroscopy (IR) has been widely used to characterize phosphates (18) and, more generally, catalyst surfaces during and following reaction. For example, the structure of disodium phosphate has been carefully characterized (19), and IR spectroscopy has been applied to study of the interaction of supported heteropoly acids with silica and silica–alumina supports (20). Experimental systems for conducting *in-situ* IR spectroscopy of catalyst surfaces (21–27) have been described.

III. METHODS

III.1. Materials and Catalyst Preparation

Lactic acid was obtained in 85% aqueous solution from Aldrich. Sodium lactate (98%) was also obtained from Aldrich as a crystalline solid, as were $NaH_2PO_4 \cdot H_2O$, Na_2HPO_4, and $Na_4P_2O_7$. Solid $Na_3PO_4 \cdot 12H_2O$ was obtained from EM Science. Solid $(NaPO_3)_n$, $Na_5P_3O_{10}$, and $Na_3P_3O_9$ (practical grades) were obtained from Sigma. Reagent grade phosphoric acid, H_3PO_4, (85% solution) was obtained from Mallinckrodt. Catalyst support (93% SiO_2, 7% Al_2O_3) was obtained from Johnson–Matthey in pellets 2.3 mm diameter $\times$ 2.3 mm in length. This support has a BET surface area of 5.1 m^2/g; its surface acidity has been characterized by pyridine adsorption (7).

As-received salts were ground with a mortar and pestle to achieve uniform consistency before heat treatment and spectroscopic analysis. Prior to use, silica–alumina support was crushed and sieved to $-30 + 60$ mesh to achieve a uniform sample for NMR spinning. Crushed supports were loaded with phosphate salts, as in our previous work (6), by wet impregnation followed by drying at 100°C overnight. Phosphate loading was 1.0 mmol phosphorus per gram support for all samples; this quantity of catalyst, if uniformly distributed on the support surface, would form a film approximately 20 monolayers thick. Prior work (6) showed no dependence of activity on phosphate loading above 0.5 mmol/g on silica–alumina, indicating a large excess of catalyst on the surface. This catalyst loading is also more than sufficient to neutralize any surface acidity of the silica–alumina support.

Following preparation, neat and supported salts were placed in crucibles in a Thermolyne 1300 furnace for heat treatment. Samples were heated for 4–6 h at specified temperatures in the range 100 to 450°C, then removed from the furnace and allowed to cool in air. Some supported catalysts were used in lactic acid conversion studies and recovered for post-reaction analyses. All samples were stored in sealed glass vials prior to analysis or use as catalysts.

III.2. NMR Methods

Sample loading. Loading a clean sample rotor was accomplished by filling with loose sample and tapping lightly on a solid surface several times to pack the sample evenly; filling and tapping were repeated until sample contacted the rotor end cap upon closing. Care was taken to clean the closed sample rotor before inserting it into the probe to avoid sample imbalance, which adversely affects results.

NMR spectrometer. MAS ^{31}P-NMR spectra were obtained at room temperature by weighted Fourier transformation of free induction decays observed by quadrature detection at 161.903 MHz. The NMR spectrometer is a Varian Model VXR-400S with an Oxford cryomagnet generating a magnetic field of 9.395 T. A Varian 400VT CP/MAS sample probe was used with a 7-mm-diameter rotor and a top speed of about 8 kHz. The computer data acquisition and analysis software was VNMR Ver. 4.1 run on a Sun workstation. Data acquisition was accomplished using a normal single pulse sequence. Operating parameters for normal data acquisition are presented in Table 2.

Chemical shift, δ, determined by reference to external calcium hydroxyapatite powder ($Ca_{10}(OH)_2(PO_4)_6$, Aldrich) at 2.8 ± 0.2 ppm, is reported according to IUPAC convention with $\delta > 0$ representing a downfield shift relative to the standard reference of 85% phosphoric acid. Typically, 32 free induction decays were collected and Fourier transformed. Chemical shifts of isotropic peaks were typically reproducible to ± 0.50 ppm; signal-to-noise ratios ranged from 40 for NaH_2PO_4 to 240 for Na_3PO_4. Peakwidths (FWHM) for the spectra cover a range from 1.05 to 18.3 ppm with a typical peakwidth of about 2.5 ppm. Errors in chemical shift values increase in broader peaks as the peak center becomes harder to identify. During operation, the instrument typically maintained a spinning frequency within ± 15 Hz of the designated frequency; spectra were collected at spinning frequencies of 4–7 kHz.

Spectra of the sodium phosphates were often complicated by the different chemical species present. For instance, heated samples of NaH_2PO_4 exhibited at least six isotropic peaks with a large anisotropy associated with four

TABLE 2

Parameters for Normal MAS ^{31}P-NMR Data Acquisition

Transmitter frequency (MHz)	161.903
Spectral width (kHz)	100
Number of data points	16,000
Acquisition time (s)	0.080
Number of scans	64
First delay, d1 (s)	10.0
Pulse width, pw (μs)	4.0

of the signals to produce intense sidebands. In this spectrum it was difficult to distinguish overlapping sidebands from isotropic peaks. Therefore, in addition to collecting MAS ^{31}P-NMR spectra at normal conditions, spectra were collected using different operating parameters or using special features of the Varian spectrometer software. These additional spectra helped to clarify the rather complicated NMR spectra of certain phosphates.

First, the spinning frequency was varied over the range 4–7 kHz to distinguish isotropic peaks from spinning sidebands. Because apparent chemical shifts of spinning sidebands are proportional to spinning frequency, sidebands change position when spinning frequency is altered and thus can be identified. To further distinguish overlapping sidebands from isotropic peaks, a method called total sideband suppression (TOSS) on the VNMR Ver. 4.1 software was implemented. This method uses a sequence of 180° pulses to induce timed spin-echoes to suppress spinning sidebands. The TOSS sequence worked well for suppression of sidebands, but typical values of S/N decreased from 27 for the standard acquisition sequence to 8.2 for the TOSS sequence.

Finally, several heteronuclear ^{31}P{^{1}H} proton decoupling experiments were performed to determine if some of the peaks observed in complicated spectra were caused by splitting of phosphorus signals due to coupling with hydrogen. Details of this method are provided by Martin *et al.* (29), and coupling constants for ^{31}P^{1}H and ^{31}P^{31}P used in the analysis are given by Emsley and Hall (30).

III.3. Infrared Methods

Species present on the catalyst surface prior to and following exposure to lactic acid were investigated by transmission FTIR spectroscopy of phosphate-coated silicon disks as model catalysts and by diffuse reflectance FTIR spectroscopy (DRIFTS) of actual supported catalysts used in lactic acid conversion.

Postreaction FTIR spectroscopy of model catalysts. To simulate the supported catalysts used in lactic acid conversion, infrared-transparent silicon disks were coated with sodium phosphate salts and exposed to lactic acid at temperatures ranging from 25 to 350°C. The treated disks were then cooled, transferred to the FTIR spectrometer, and analyzed via transmission FTIR to identify surface species present on the quenched catalyst following reaction. This method provides rapid and reliable collection of IR spectra of surface species present on the phosphate catalysts following reaction.

Silicon IR disks (9 mm × 2 mm, Spectra Tech, Inc.) were chosen as model catalyst supports because of their durability and wide IR-transparent window (8300 to 660 cm^{-1}). The thin silicon oxide layer on the disk surface also makes it a reasonable representation of the actual catalyst support used. Disks were placed in clip-style holders securing the disk by its edges, and 25 μl of an aqueous solution containing 3.7×10^{-6} M phosphate salt or organic species was pipetted onto each side of the disk. The disk was then carefully dried at room temperature in a dessicator under controlled vacuum. This process was then repeated so that a total of 100 μl were placed on the disk; this quantity of material provides appropriate transmittance in the spectrometer.

After vacuum drying, the sample disk was removed from the clip-style holder and placed in the apparatus described below for exposure to lactic acid or placed in a magnetic sample holder for analysis in the spectrometer. Exposure to air was kept to an absolute minimum to avoid absorption of moisture.

A bench-top glass apparatus (Fig. 2) was constructed to expose prepared sample disks to lactic acid vapor at temperatures from 100 to 350°C. The 200 ml round bottom flask has necks for a thermocouple and helium carrier gas inlet along with the vertical column where the sample disk is located. The round bottom flask, which contains a solution of lactic acid, is heated on the bottom by a heating mantle and around the top by heating tape. The column and distilling head are heated with heating tapes independently of the flask, so that the column and flask temperature are controlled separately. Exterior tubing for the apparatus is designed to allow helium carrier gas flow in either direction through the apparatus. Effluent flow rate is measured through a bubblemeter.

The apparatus was prepared for experiment by adding 100 ml of 85% aqueous lactic acid solution to the round bottom flask, and then driving off the water in solution by heating the flask at 140°C for 1 h under 500 ml/min helium. The column was heated to 160°C during this time to prevent lactic acid condensation prior to insertion of the disk. After water removal, the column was heated to the desired temperature for exposure to lactic acid. The sample disk was inserted by reversing the helium flow direction to direct lactic acid away from the column, removing the distilling head from the column, and placing the disk on the glass frit inside the column. The distilling head was then replaced as quickly as possible and the column was allowed to return to the desired temperature. Upon reaching steady state, helium flow was turned to the forward direction and the disk exposed to lactic acid vapors for 10 min. Helium flow was then reversed once again to avoid further exposure to lactic acid, the column was cooled to about 100°C, and the sample disk was removed and analyzed by transmission FTIR.

A Nicolet IR/42 spectrometer with a deuterated triglycine sulfate (DTGS) pyroelectric detector was used for transmission FTIR spectroscopy. Spectra were collected in the mid-IR region 400–4800 cm^{-1} with a resolution of 4 cm^{-1}. Typical spectral collection included first the collection of a background spectrum in the empty spectrometer

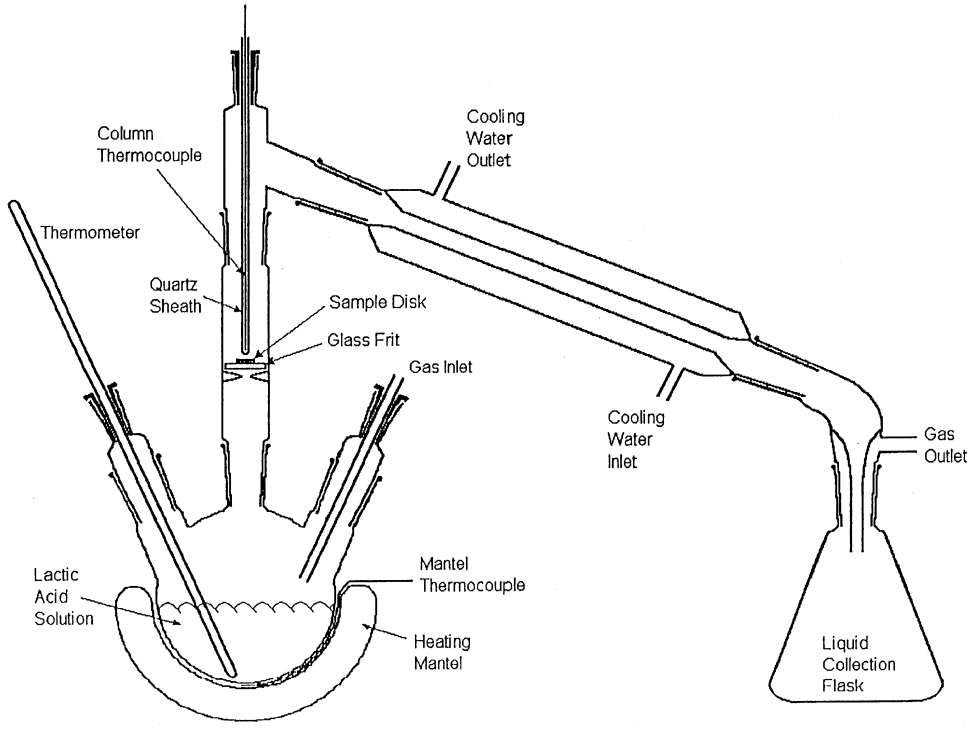

FIG. 2. Apparatus for preparing sample disks for postreaction FTIR analysis.

sample compartment, then collection of a reference spectrum using the clean silicon disk prior to preparation and exposure to lactic acid, and finally collection of the spectrum of the catalyst-loaded disk following exposure to lactic acid. In collecting spectra, exposure to air was minimized and the spectrometer sample compartment was purged with nitrogen to avoid adsorption of moisture. Following collection of spectra, the reference spectrum was subtracted. Reproducibility of sample preparation and spectroscopic techniques was confirmed by comparing repeated experiments: absorption frequencies of major peaks usually agree to within the 4 cm^{-1} resolution used.

Postreaction DRIFTS of supported catalysts. Selected phosphate catalysts supported on silica/alumina were analyzed by diffuse reflectance IR spectroscopy following use in lactic acid conversion studies in the bench-scale laboratory reactor described previously (6). Supported catalysts were mixed with KBr to make a sample containing 10 wt% catalyst; this mixture was loaded into a microsample cup in a Mattson Galaxy 3000 FTIR spectrometer equipped with a SpectraTech DRIFTS attachment. The FTIR spectrum was collected by taking 100 scans at 4 cm^{-1} resolution. The background spectrum for DRIFTS was taken as that of the silica/alumina support in KBr at the same concentration, so that the spectra reported represent only the phosphate catalyst and organic surface species present.

IV. RESULTS

IV.1. ^{31}P-NMR Analysis of Phosphate Thermal Transformations

Thermal transformations of the three orthophosphate salts, both neat and supported on silica/alumina, are reported here via MAS ^{31}P-NMR spectroscopy at room temperature or following heating at 100, at 300, and at 450°C. The species represented in the spectra are those present in the catalyst at the onset of lactic acid conversion. Key results are reported here, with additional spectra and further analyses given elsewhere (31). Spinning frequency (ν) for each sample is noted in the figures.

NaH_2PO_4. The MAS ^{31}P-NMR spectra describing thermal transformations of monosodium phosphate are shown in Fig. 3. The as-received material exhibits a single isotropic chemical shift at 1.8 ± 0.4 ppm (Fig. 3a), close to the literature value of 2.3 ppm (14). Following heat treatment at 300°C for 4 h in air, isotropic peaks appear at 2.0, −8.3, −15.6, −19.4, −24.1, and −26.3 ppm (Fig. 3b). Analysis by spinning frequency variation (Fig. 3c) and TOSS (Fig. 3d) confirm that these six peaks are unique signals and are not spinning sidebands. The isotropic peaks are not the most intense peaks in the spectrum; furthermore, the TOSS method is not completely effective in eliminating sidebands relative to the isotropic peaks. After heat treatment to 450°C, five isotropic peaks are observed at −5.4, −15.3,

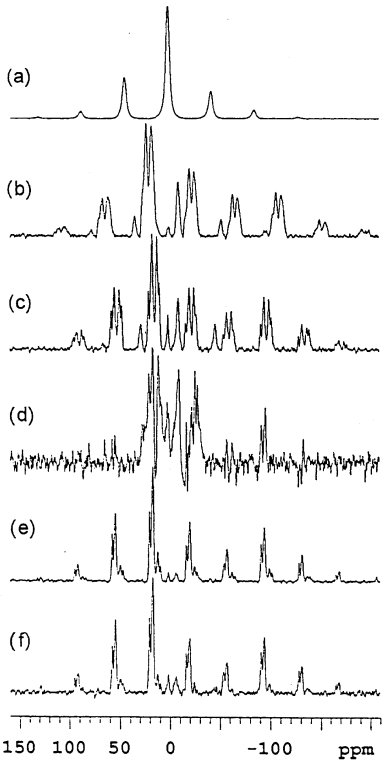

FIG. 3. MAS ^{31}P-NMR spectra of NaH_2PO_4: (a) 25°C, $\nu = 7$ kHz; (b) 300°C, $\nu = 7$ kHz; (c) 300°C, $\nu = 6$ kHz; (d) 300°C, $\nu = 6$ kHz, TOSS; (e) 450°C, $\nu = 6$ kHz; (f) 450°C, $\nu = 6$ kHz, ^{31}P{^{1}H} decoupling in effect.

−19.0, −24.0, and −26.2 ppm (Fig 3e). ^{31}P{^{1}H} proton decoupling (Fig. 3f) has no effect on the spectrum, indicating no substantial ^{31}P^{1}H coupling.

Peaks at −15.3, −19.0, −24.0, and −26.2 ppm are assigned to linear sodium polyphosphate, $(NaPO_3)_n$ in a crystalline form, as reported by Prabhakar *et al.* (13) and others (12, 17). The decrease in the NaH_2PO_4 peak at 2.0 ppm as temperature increases indicates conversion of NaH_2PO_4. The peak at −5.4 ppm observed at 450°C has been attributed (12) to end-chain PO_4 groups; the relatively high intensity of this end-chain peak suggests that the polyphosphate chains are short. The −5.4 ppm peak may also be evidence of the presence of a small quantity of the trimeric ring, sodium trimetaphosphate ($Na_3P_3O_9$) (see Discussion).

The NMR spectra of NaH_2PO_4 supported on silica–alumina (Fig. 4) are less well-resolved than those of the pure material. Following drying at 100°C, isotropic peaks are observed at 2.4 and −5.9 ppm (Fig. 4a) which are assigned to $NaH_2PO_4 \cdot H_2O$ and $Na_3P_3O_9$, respectively. Heating to 300°C gives rise to two broad isotropic peaks at chemical shifts of −8.8 and −19.5 ppm (Fig. 4b); other peaks are confirmed as spinning sidebands by spinning frequency variation and TOSS analysis (not shown). The peak at −19.5 ppm is consistent with that for amorphous polyphosphate $(NaPO_3)_n$ (12). After heat treatment at 450°C, a broad (FWHM 18 ppm) isotropic peak, centered at −12 ppm, is observed (Fig. 4c); the noisy spectrum and large anisotropy make it difficult to determine whether there is one signal or several signals in close proximity. The peak shapes, along with ^{31}P{^{1}H} decoupling (Fig. 4d), suggest that more than one peak is present and that some hydrogen bonding with surface silanols may be occurring. The spectrum is consistent with a mixture of $Na_3P_3O_9$ (−5.9 ppm) and amorphous polyphosphate (−19.5 ppm) on the support surface.

Na_2HPO_4. The NMR spectrum of disodium orthophosphate has a single isotropic peak at 6.3 ppm (Fig. 5a), close to the literature value (14). After heating to 300°C (Fig. 5b), an isotropic peak at 1.9 ppm is observed which is assigned (12) to anhydrous tetrasodium pyrophosphate ($Na_4P_2O_7$). Variation of spinning frequency (not shown) confirms that the other bands in the pyrophosphate spectrum are spinning sidebands. Supported Na_2HPO_4 undergoes the same transformations as the pure sample: following drying at 100°C (Fig. 5c), some pyrophosphate is seen (1.3 ppm) in addition to Na_2HPO_4 (6.3 ppm). Complete conversion to pyrophosphate is observed by 300°C (Fig. 5d); the spectrum of a standard sample of $Na_4P_2O_7$ is given in Fig. 5e.

Na_3PO_4. The NMR spectrum of $Na_3PO_4 \cdot 12H_2O$ (Fig. 6a) shows one isotropic peak at 7.5–7.9 ppm, in good agreement with the literature (12, 14). The only transformation observed upon calcination of $Na_3PO_4 \cdot 12H_2O$ is dehydration. By 300°C, complete dehydration has occurred as indicated by a single peak at 14.2 ppm (Fig. 6b). Supported samples of Na_3PO_4 show the same behavior (Figs. 5c and 5d), with dehydration nearly complete at 100°C. Figure 6e is the post-reaction spectrum for supported Na_3PO_4 (see below).

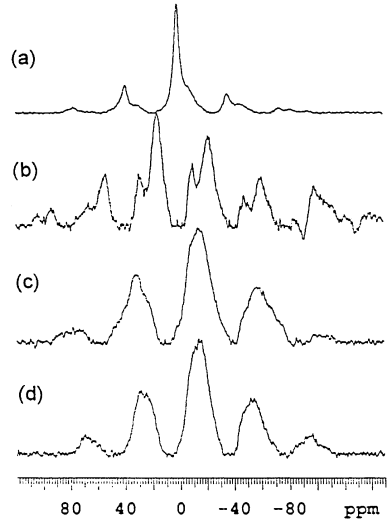

FIG. 4. MAS ^{31}P-NMR spectra of NaH_2PO_4 on silica/alumina support: (a) 100°C, $\nu = 7$ kHz; (b) 300°C, $\nu = 7$ kHz; (c) 450°C, $\nu = 6$ kHz; (d) 450°C, $\nu = 6$ kHz, ^{31}P{^{1}H} decoupling in effect.

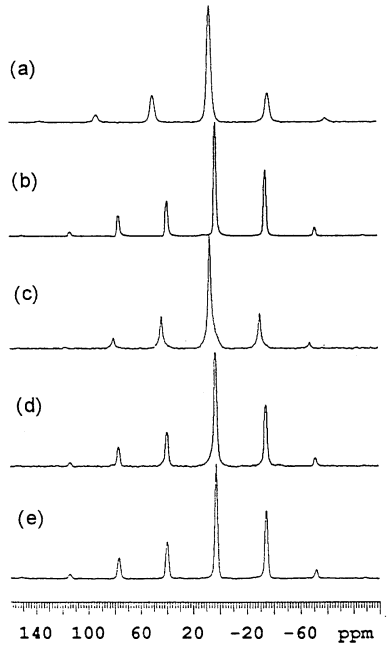

FIG. 5. MAS ^{31}P-NMR spectra of Na_2HPO_4: (a) 25°C, $\nu = 7$ kHz; (b) 300°C, $\nu = 6$ kHz; (c) on silica/alumina support, 100°C, $\nu = 6$ kHz; (d) on silica/alumina support, 300°C, $\nu = 6$ kHz; (e) $Na_4P_2O_7$ reference sample, 25°C, $\nu = 6$ kHz.

IV.2. Postreaction FTIR and ^{31}P-NMR Spectroscopy of Phosphate Catalysts

Pure component IR spectra. To determine the reliability of IR spectra taken of species on the silicon disks, spectra of lactic acid, its sodium salt, and several sodium phosphates were collected by drying a solution of the desired species on a silicon disk and then placing the disk in the IR spectrometer.

Lactic acid and sodium lactate spectra are given in Fig. 7; these spectra are consistent with band locations and intensities assigned in the literature (18). The most notable features of the spectra are the strong carbonyl stretching band (νC=O) at 1728 cm^{-1} for lactic acid and 1591 cm^{-1} for sodium lactate. Other identifying features include a strong bending–stretching band at 1221 cm^{-1} for lactic acid, and a "fingerprint" of six peaks at 1265, 1314, 1364, 1422, 1456, and 1473 cm^{-1} for sodium lactate.

Spectra for sodium orthophosphates are given in Fig. 8. All orthophosphates have a strong PO_3 asymmetric stretching frequency at 1015–1080 cm^{-1} and a less intense band attributed to PO_3 bending at 475–580 cm^{-1}. The IR spectra of several condensed sodium phosphates (Fig. 9) include bands of moderate strength in the 800–1300 cm^{-1} region and the PO_3 bending mode at 480–550 cm^{-1}. The observed bands for all phosphates agree to within ±5–10 cm^{-1} of assigned literature values (19, 20).

Postreaction FTIR spectroscopy of model catalysts. The IR spectra of surface species on phosphate-loaded silicon disks following exposure to lactic acid at 100 to 350°C are given in Figs. 10–13. Each spectrum in the figures represents a separate experiment in which a fresh sample of phosphate was deposited on a clean disk and exposed to lactic acid only at the specified temperature. The spectrum at 25°C in each figure is for an equimolar solution of lactic acid and the phosphate salt deposited on the disk and then dried at 25°C.

Monosodium phosphate (Fig. 10) exhibits no proton transfer from lactic acid in solution at 25°C; the spectrum at 25°C shows bands for both lactic acid (1715, 1476, 1130, 1048 cm^{-1}) and NaH_2PO_4 (1130, 1050, 960, 509 cm^{-1}) but no sodium lactate or phosphoric acid. At elevated temperatures evidence of lactic acid on the surface is observed (1744, 1458, 1215, 1130 cm^{-1}) only at 100°C, probably from simple condensation. The carbonyl stretch band at 100°C is shifted to 1744 cm^{-1}; this effect was reproducible in duplicate experiments and will be discussed in a

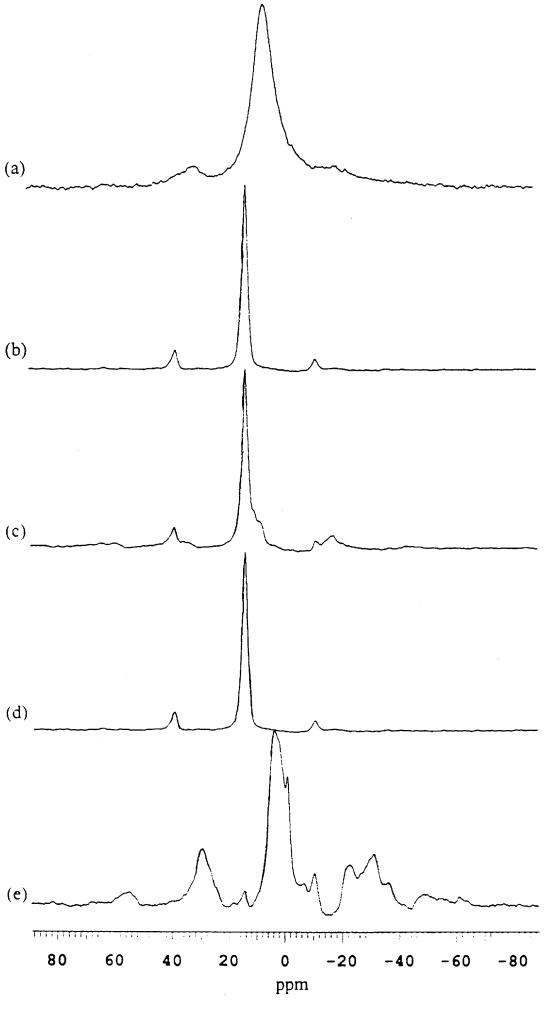

FIG. 6. MAS ^{31}P-NMR spectra of $Na_3PO_4 \cdot 12H_2O$: (a) 25°C, $\nu = 4$ kHz; (b) 450°C, $\nu = 4$ kHz; (c) on silica/aumina support, 100°C, $\nu = 4$ kHz; (d) on silica/alumina support, 450°C, $\nu = 4$ kHz; (e) on silica/alumina support following lactic acid conversion at 320°C, $\nu = 4$ kHz.

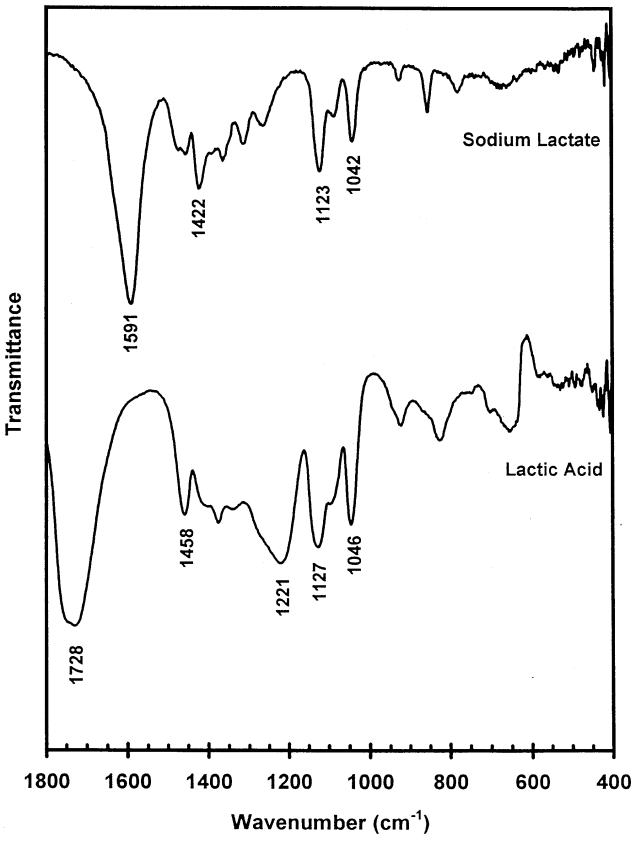

FIG. 7. FTIR spectra of sodium lactate and lactic acid deposited on silicon disk.

forthcoming paper. At 200°C and above, sodium polyphosphate $(NaPO_3)_n$ becomes the dominant species on the surface (1270, 1092, 870, 705, 490 cm^{-1}). There are bands at ≈1300 and 1163 cm^{-1} which suggest the presence of sodium trimetaphosphate ($Na_3P_3O_9$), but other metaphosphate bands at 988, 760, and 517 cm^{-1} are not present. It is possible that another organic species is present on the surface at 200–350°C.

Disodium phosphate (Fig. 11) shows significant proton transfer from lactic acid in solution at 25°C and upon exposure to lactic acid vapors at 100°C. At both temperatures, the spectrum shows a mixture of lactic acid, sodium lactate, Na_2HPO_4, and NaH_2PO_4. Spectra at 150 and 200°C show sharp peaks at 857 and 541 cm^{-1} consistent with Na_2HPO_4, but peaks at 1142 and 1057 cm^{-1} suggest that partial dehydration has taken place and a stable intermediate is present. Above 200°C, dehydration of Na_2HPO_4 to sodium pyrophosphate ($Na_4P_2O_7$) is complete as evidenced by the strong absorption band at 1123 cm^{-1}. At 200°C and above, the carbonyl band at 1599 cm^{-1} indicates that sodium lactate forms as a result of proton transfer from lactic acid to tetrasodium pyrophosphate.

Trisodium phosphate dodecahydrate (Fig. 12) completely deprotonates lactic acid upon mixing in solution at 25°C, giving the spectrum of sodium lactate and Na_2HPO_4. Upon exposure to lactic acid vapors at 100 or 150°C, lactic acid is seen along with sodium lactate and disodium phosphate. The lactic acid carbonyl stretch is again shifted to 1740 cm^{-1}. At 200°C and above, the presence of sodium lactate (1599 cm^{-1}) and $Na_4P_2O_7$ (570, 920, 1127 cm^{-1}) indicates proton transfer is occurring on the catalyst surface to form sodium lactate and Na_2HPO_4, which then condenses to the pyrophosphate. The bands at 570 and 920 cm^{-1} are shifted somewhat from those reported for $Na_4P_2O_7$ in the literature.

To corroborate the observed behavior for orthophosphates, FTIR spectra of $Na_4P_2O_7$ exposed to lactic acid at various temperatures are given in Fig. 13. High concentrations of lactic acid on the disk complicate the spectra at low temperatures, but sodium lactate, which can only be formed by proton transfer to pyrophosphate, is clearly present (C=O stretch at 1600 cm^{-1}) at 150°C and above. Sodium lactate and $Na_4P_2O_7/Na_3HP_2O_7$ (1123 cm^{-1}) are the dominant species present at these temperatures, in agreement with results obtained for di- and trisodium phosphates.

Postreaction DRIFTS and ^{31}P-NMR analyses of supported Na_3PO_4. To verify that phosphates on the silicon disks are reasonable representations of actual supported catalysts, postreaction ^{31}P-NMR and DRIFTS of silica/alumina-

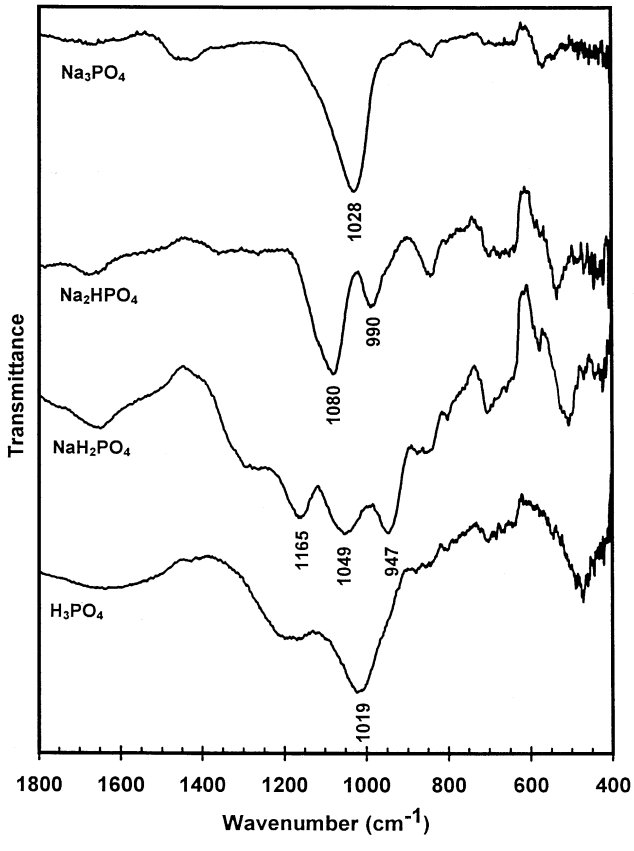

FIG. 8. FTIR spectra of orthophosphates deposited on silicon disk.

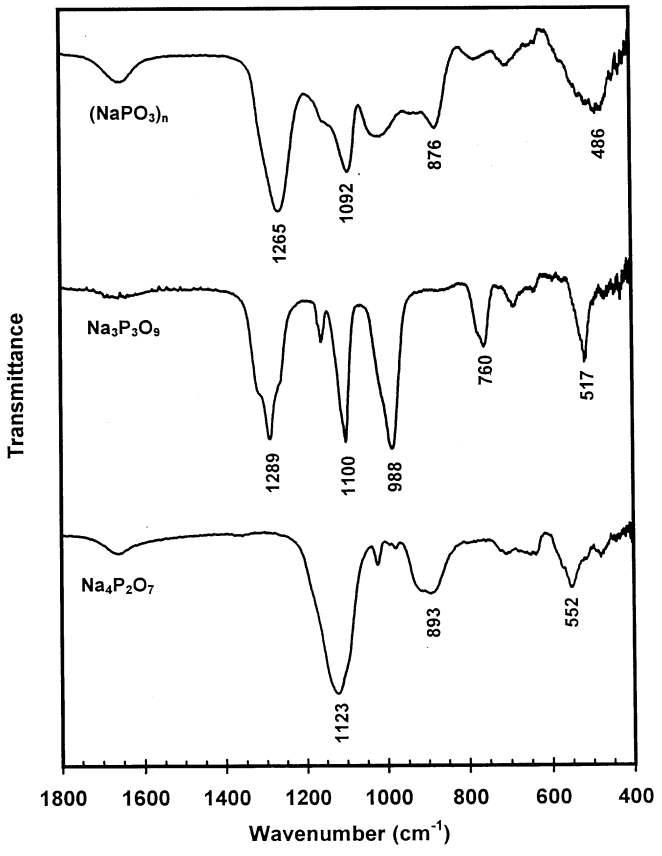

FIG. 9. FTIR spectra of condensed phosphates deposited on silicon disk.

supported trisodium phosphate catalysts used in lactic acid conversion studies were conducted. The ^{31}P-NMR spectrum (Fig. 6e) shows five isotropic peaks at 3.2, 0.7, −0.6, −6.8, and −10.0 ppm. The primary species present are anhydrous $Na_4P_2O_7$ (3.2 ppm) and $Na_4P_2O_7 \cdot 10H_2O$ (−0.6 ppm). The peaks for these species are shifted slightly from those in Fig. 5 but are within the ranges given by Hayashi *et al.* (12). The peaks at 0.7 and −6.8 ppm are assigned to anhydrous sodium triphosphate ($Na_5P_3O_{10}$), and the peak at −10.0 ppm is tentatively assigned to hydrated triphosphate ($Na_5P_3O_{10} \cdot xH_2O$). The shift in the peak from that of the anhydrous triphosphate (at −6.8 ppm) is similar to that observed upon hydration of other phosphates. The linear triphosphate is believed to form by condensation of the proton exchange products $Na_3HP_2O_7$ and Na_2HPO_4.

The DRIFTS spectrum of supported trisodium phosphate catalyst is given in (Fig. 14a). The presence of sodium lactate (1578 and 1418 cm^{-1}) and tetrasodium pyrophosphate (1120 cm^{-1}) on the supported catalyst is verified, in agreement with results obtained on silicon disks. The DRIFTS spectrum of Na_3PO_4 on silica/alumina prior to reaction (Fig. 14b) and the spectrum of neat Na_3PO_4 (Fig. 14c) are also shown. Both of these DRIFTS spectra are in agreement with the transmission FTIR spectra collected on the silicon disks, further supporting the validity of the methods used in this work.

V. DISCUSSION

Infrared and NMR results of this study reveal that supported sodium phosphates undergo thermal transformations consistent with those of neat sodium phosphates (8, 30, 32). Our NMR results for NaH_2PO_4 condensation agree with the literature (33) in formation of $Na_3P_3O_9$ or $(NaPO_3)_n$ at high temperatures, but our spectra differ somewhat for neat and supported salts in that we believe we see a mixture of $Na_3P_3O_9$ and $(NaPO_3)_n$ on the support and only $(NaPO_3)_n$ for the neat salt. This is reasonable; on the support, NaH_2PO_4 is likely in a more dispersed state than the neat salt, so that smaller condensation products such as trimetaphosphate (trimer) are favored over polyphosphate (linear polymer). Phosphate anions may also interact with acidic surface sites on the silica–alumina support (7), further inhibiting formation of long chains. The broad peaks for supported NaH_2PO_4 make more in-depth analysis difficult.

For neat NaH_2PO_4 at 300°C, a peak at −8 to −9 ppm, which has been attributed (10–12, 16, 34) only to the central phosphorus atom of linear triphosphate ($Na_5P_3O_{10}$) is

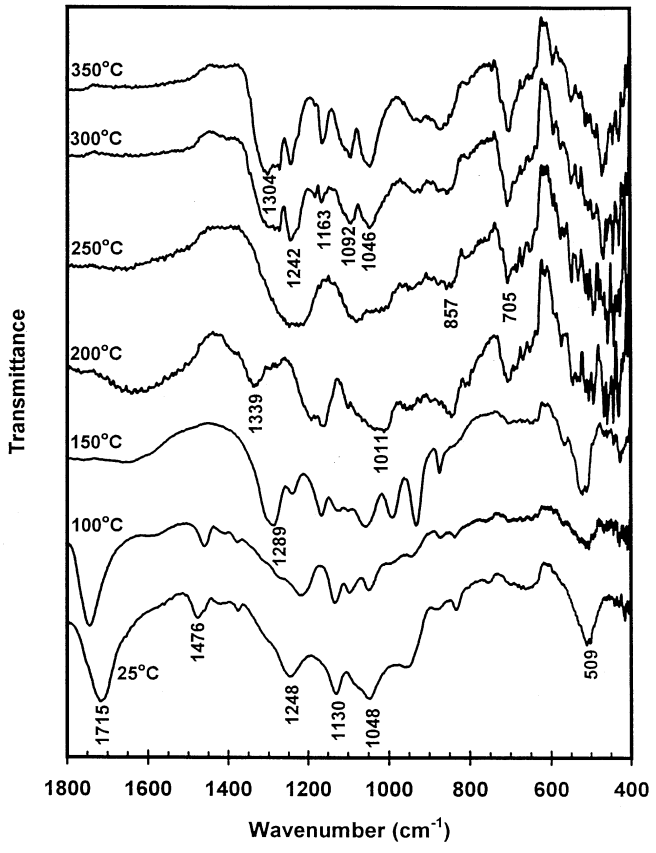

FIG. 10. Postreaction FTIR spectra of NaH_2PO_4 deposited on silicon disk and exposed to lactic acid at different temperatures.

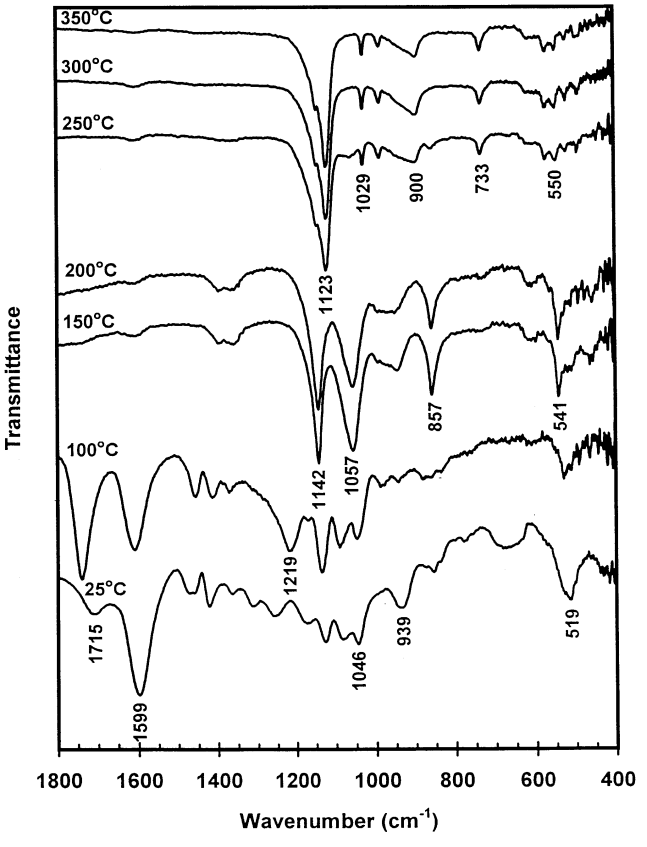

FIG. 11. Postreaction FTIR spectra of Na_2HPO_4 deposited on silicon disk and exposed to lactic acid at different temperatures.

observed. We do not believe that $Na_5P_3O_{10}$ is present, because we do not observe the peak for its terminal phosphate atom at 1.2 ppm, and because it is not the stoichiometric condensation product of NaH_2PO_4. The source of the peak at −8 to −9 ppm in the NMR spectra of NaH_2PO_4 at 300°C is not understood at this time.

Postreaction FTIR spectroscopy shows that proton transfer from lactic acid to sodium phosphate leads to sodium lactate as a stable species on the catalyst surface during reaction. Proton transfer was observed with Na_3PO_4 and $Na_4P_2O_7$ at all temperatures, with Na_2HPO_4 at 25 and 100°C (before it transforms to pyrophosphate), and not at all with NaH_2PO_4. This behavior is consistent with the relative acidities of lactic acid ($pK_a = 3.86$ at 25°C), phosphoric acid ($pK_{a1} = 2.1$; $pK_{a2} = 7.2$; $pK_{a3} = 12.4$ at 25°C) (33) and pyrophosphoric acid ($H_4P_2O_7$, $pK_{a1} = 1.5$, $pK_{a2} = 2.36$, $pK_{a3} = 6.6$, $pK_{a4} = 9.25$ at 25°C) (33, 35). For example, HPO_4^{2-} and $H_2PO_4^-$ are weaker acids than lactic acid and therefore retain protons better, so that lactate exists in its ionic form in their presence. The converse is true with H_3PO_4, so that lactate exists as undissociated lactic acid with monosodium phosphate catalyst. Solution equilibrium calculations at 25°C verify that quantitative proton transfer occurs where it is favored.

Results of spectroscopic analyses on both model and actual catalysts provide insight into the catalytic action of the phosphate salts as reported in Table 1. First, there is a definite correspondence between the presence of both pyrophosphate and sodium lactate on the catalyst surface and catalytic activity toward acrylic acid and 2,3-pentanedione formation. Product selectivities over disodium and trisodium phosphate are the same within experimental uncertainty at 300 and 350°C. Lactic acid conversion is the same over the two salts at 300°C but higher over trisodium phosphate at 350°C. We have also verified that starting with $Na_4P_2O_7$ as the catalyst gives the same product selectivities as conversion starting with disodium orthophosphate. The IR spectra (Figs. 11–14) of all of these catalysts indicate the presence of both pyrophosphate and sodium lactate. In contrast, condensed phosphates from NaH_2PO_4 have essentially no catalytic activity for 2,3-pentanedione or acrylic acid formation, and post-reaction IR indicates no sodium lactate present on the surface (Fig. 10). In fact, relative to the support alone, the only positive aspect of adding monosodium phosphate is the reduced formation of undesirable byproduct acetaldehyde via neutralization of acidic support sites.

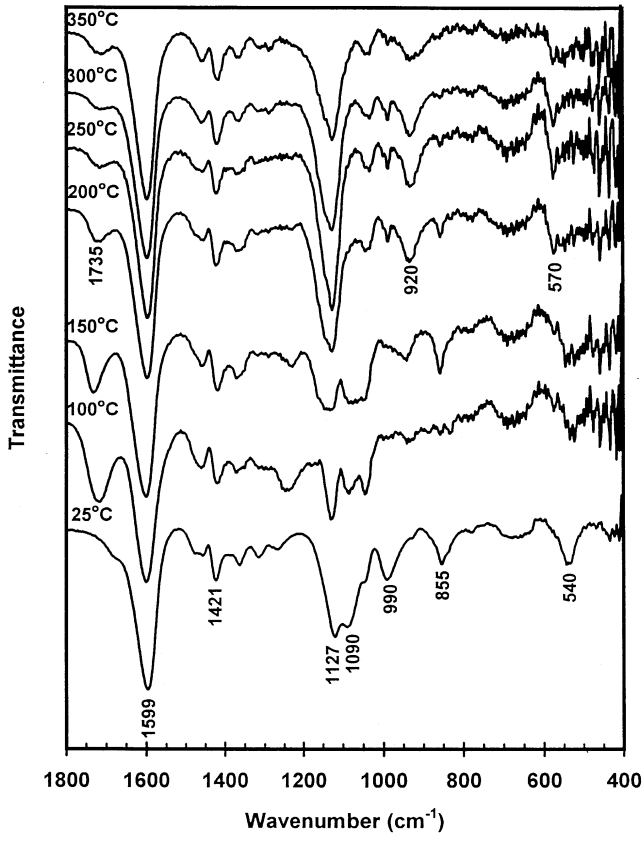

FIG. 12. Postreaction FTIR spectra of Na_3PO_4 deposited on silicon disk and exposed to lactic acid at different temperatures.

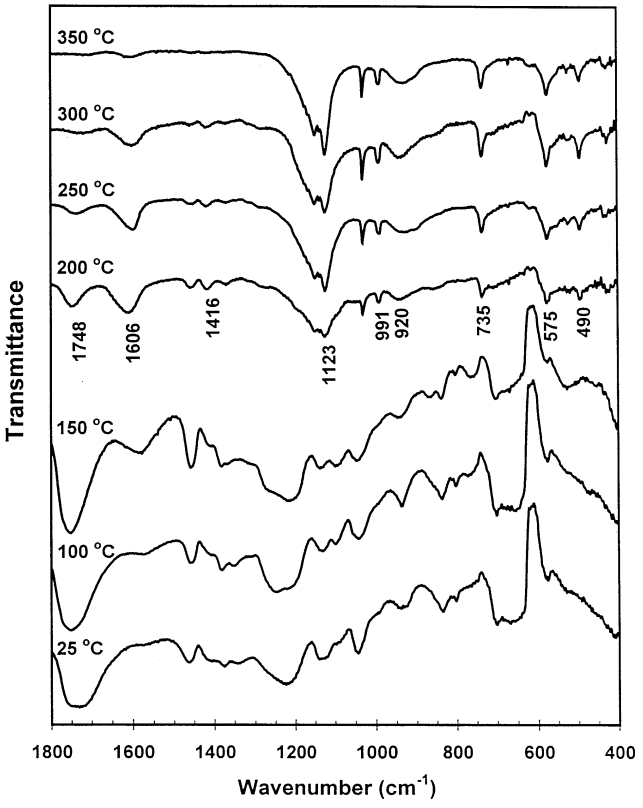

FIG. 13. Postreaction FTIR spectra of $Na_4P_2O_7$ deposited on silicon disk and exposed to lactic acid at different temperatures.

We have proposed a modified Claisen condensation of two lactate moieties as the route to 2,3-pentanedione formation from lactic acid (6). The results obtained here suggest that sodium lactate is an intermediate in 2,3-pentanedione formation, as the mechanism can be written with one or both lactate groups as anions. To test this, we duplicated the composition of the catalyst surface in a bulk, condensed-phase experiment by mixing sodium lactate (Aldrich, 99.5%) with $Na_4P_2O_7$ with a 2 : 1 molar ratio and then slowly heating the mixture to 350°C in flowing helium in a small reaction cell. We observed no formation of 2,3-pentanedione or acrylic acid and only a very small quantity of acetaldehyde in the trapped effluent. We repeated the experiment with only sodium lactate and obtained similar results. These experiments indicate that sodium lactate alone or in the presence of pyrophosphate does not form 2,3-pentanedione.

Based on the above condensed-phase attempt at 2,3-pentanedione formation, we conclude that sodium lactate must condense with free lactic acid to form the diketone if it is an intermediate in the reaction pathway. It is also possible that sodium lactate is not an intermediate but a catalyst, either acting by itself or in conjunction with pyrophosphate. Our related work (7) with other sodium salts suggests that the presence of lactate alone on the support can lead to 2,3-pentanedione formation from lactic acid, but at this time we cannot differentiate between its possible roles as a catalyst or as an intermediate.

If relative IR peak intensities in Figs. 11–13 are taken as a relative measure of sodium lactate and pyrophosphate concentrations, a much greater extent of proton transfer was observed for Na_3PO_4 than for $Na_4P_2O_7$ and Na_2HPO_4. The large quantity of sodium lactate on the trisodium phosphate catalyst surface may explain the higher activity of Na_3PO_4 relative to Na_2HPO_4 at low temperature (Table 1), although this is not the case at the higher temperature where activities are the same. Conversion at higher temperatures is obviously affected by something other than quantity of sodium lactate present on the surface.

At first, the lesser extent of proton transfer to $Na_4P_2O_7$ is puzzling, because pK_a values indicate that pyrophosphoric acid is as favorable for proton transfer as orthophosphoric acid. However, there are several factors which may limit the extent of proton transfer to pyrophosphate relative to trisodium orthophosphate. First, pyrophosphate is stable on the catalyst surface at reaction conditions, so that reverse proton exchange to reform lactic acid can occur. Trisodium hydrogen pyrophosphate forms when proton exchange

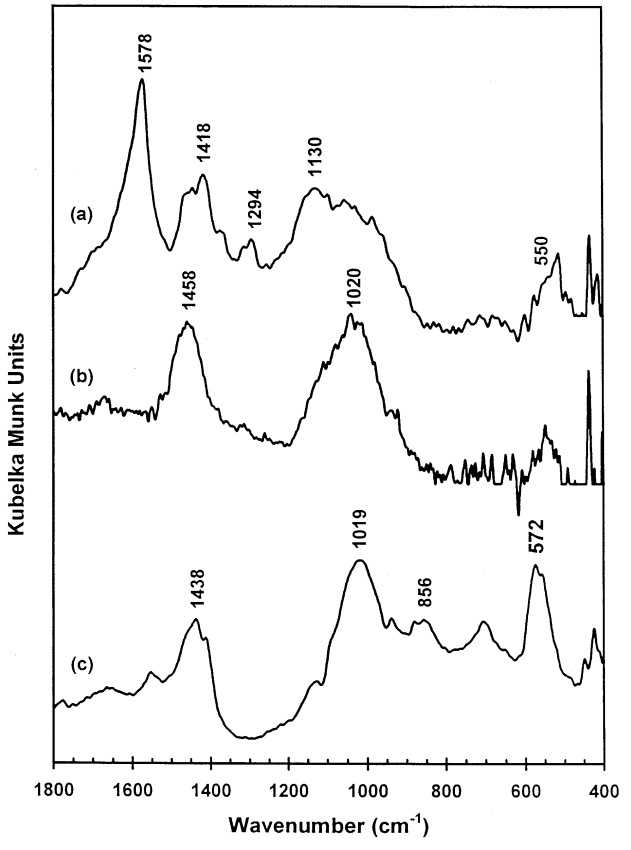

FIG. 14. DRIFTS spectra: (a) Na_3PO_4 supported on silica/alumina following lactic acid conversion at 320°C; (b) Na_3PO_4 supported on silica alumina prior to conversion; (c) neat Na_3PO_4.

occurs with pyrophosphate; we cannot observe this species but we do see sodium lactate as evidence of the exchange. We also observe a small amount of sodium triphosphate ($Na_5P_3O_{10}$) via postreaction ^{31}P-NMR analysis; the triphosphate forms via condensation of $Na_3HP_2O_7$ and Na_2HPO_4 and is thus evidence of proton transfer with pyrophosphate (as is sodium lactate formation). Nevertheless, pyrophosphate is still the dominant species on the surface and reverse proton exchange can in principle occur to recover the starting species. In contrast, proton transfer to the orthophosphate is irreversible in that the disodium salt condenses rapidly to pyrophosphate as it is formed, expelling the acid protons in product water. Once formed, sodium lactate cannot reexchange a proton from the phosphate, and proton transfer proceeds to completion. We do not believe that water present in lactic acid conversion can hydrolyze the pyrophosphate-sodium lactate mixture back to disodium orthophosphate at reaction conditions. To check this, we calcined used Na_3PO_4 catalyst overnight at 450°C in air and then took the ^{31}P-NMR spectrum; only partially regeneration of trisodium phosphate was observed even under these extreme conditions.

Second, the extent of sodium dissociation from phosphate anions, while over 90% for orthophosphates, decreases with increasing chain length for condensed phosphates (36). Incomplete sodium dissociation from $P_2O_7^{4-}$ would lead to relatively stronger acids than lactic acid, which would in turn suppress proton transfer. Nevertheless, for pyrophosphate at least, sodium dissociation appears to approach 75% (36), so that the resulting base is still strong enough to transfer a proton from lactic acid. Again, calculation at 25°C verifies this.

Third, it is reasonable to assume that proton transfer is expedited by the presence of a liquid phase on the catalyst surface. Below 100°C, liquid water is likely present, and proton transfer is observed on all but monosodium phosphate catalyst. At higher temperatures, complete proton transfer between Na_3PO_4 and lactic acid is consistent with a liquid phase of some kind on the support surface. We used the dodecahydrate ($Na_3PO_4 \cdot 12H_2O$) as the starting material for Na_3PO_4 catalyst; this compound is not pure Na_3PO_4 but is a solid solution of approximate composition $Na_3PO_4 \cdot 1/7NaOH \cdot 12H_2O$ with a Na/P ratio of about 3.2 (37). Upon heating this material, a series of Na_3PO_4 hydrates are observed along with NaOH, with anhydrous Na_3PO_4 (m.p. 1340°C) forming above 210°C (38). It is likely that NaOH (m.p. 308°C) exists as a hydrated liquid phase on the support surface at reaction conditions and that proton transfer from lactic acid occurs in this phase. Further, sodium lactate exists in a molten state at reaction temperatures, and will increase the quantity of liquid phase present as it is formed. Trisodium phosphate itself will not be present as a liquid at elevated temperatures in the presence of water vapor; Na_3PO_4 solubility in water declines sharply above 210°C where the anhydrous salt is in equilibrium with solution (39).

In contrast to the trisodium phosphate catalyst, there may be no liquid phase present to enhance proton transfer to $Na_4P_2O_7$ (or the condensed phosphates $(NaPO_3)_n$) because they exist as anhydrous solids above 250°C (33, 40). Thus proton transfer from lactic acid, although it does appear to occur with pyrophosphate, is limited in the absence of a fluid surface phase.

In conclusion, we have demonstrated here a relationship between the presence of sodium lactate and sodium pyrophosphate on the catalyst surface and catalytic activity toward 2,3-pentanedione and acrylic acid formation. Catalyst activity is improved by increased quantity of sodium lactate on the surface at low temperatures, but the effect is not seen at high temperatures. We cannot determine at this time if sodium lactate is a catalyst for or an intermediate in 2,3-pentanedione formation, but thermal decomposition of sodium lactate alone does not give 2,3-pentanedione. We are continuing our efforts to better understand the active catalyst species on the surface.

ACKNOWLEDGMENTS

The support of the United States Department of Agriculture, National Research Initiative Competitive Grants Program, through Award 93-37500-9585 is appreciated. Support of the Crop and Food Bioprocessing Center, State of Michigan Research Excellence Fund, is also acknowledged. NMR data were collected on instrumentation purchased in part with funds from NIH Grant 1-S10- RR04750, NSF Grant CHE-88-00770, and NSF Grant CHE-92-13241.

REFERENCES

1. Holmen, R. E., U.S. Patent 2,859,240 (1958).
2. Paparizos, C., Dolhyj, S. R., and Shaw, W. G., U.S. Patent 4,786,756 (1988).
3. Sawicki, R. A., U.S. Patent 4,729,978 (1988).
4. Mok, W. S., Antal, M. J., Jr., and Jones, M., Jr., *J. Org. Chem.* **54**, 4596 (1989).
5. Lira, C. T., and McCrackin, P. J., *Ind. Eng. Chem. Res.* **32**, 2608 (1993).
6. Gunter, G. C., Jackson, J. E., and Miller, D. J., *J. Catal.* **148**, 252 (1994).
7. Langford, R. E., Gunter, G. C., Jackson, J. E., and Miller, D. J., *Ind. Eng. Chem. Res.* **34**, 974 (1995).
8. Greenfield, S., and Clift, M., "Analytical Chemistry of the Condensed Phosphates." Pergamon, New York, 1975.
9. Hudson, R. B., and Dolan, M. J., *in* "Kirk–Othmer Encyclopedia of Chemical Technology" (M. Grayson, Ed.), 3rd ed., Vol. 17, p. 426. Wiley, New York, 1968.
10. Andrew, E. R., Bryant, D. J., Cashell, E. M., and Dunell, B. A., *Chem. Phys. Lett.* **77**(3), 614 (1981).
11. Burlinson, N. E., Dunell, B. A., and Ripmeester, J. A., *J. Magn. Reson.* **67**, 217 (1986).
12. Hayashi, S., and Hayamizu, K., *Bull. Chem. Soc. Jpn.* **62**, 3061 (1989).
13. Prabhakar, S., Rao, J. K., and Rao, C. N. R., *Chem. Phys. Lett.* **139**(1), 96 (1987).
14. Turner, G. L., Smith, K. A., Kirkpatrick, R. J., and Oldfield, E., *J. Magn. Res.* **70**, 408 (1986).
15. Herzfeld, J., and Berger, A. E., *J. Chem. Phys.* **73**(12), 6021 (1980).
16. Un, S., and Klein, M. P., *J. Am. Chem. Soc.* **111**, 5119 (1989).

17. Duncan, T. M., and Douglass, D. C., *Chem. Phys.* **87**, 339 (1984).
18. Simons, W. M., Ed., "The Infrared Spectra Handbook of Inorganic Compounds." Sadtler Research Labs, Philadelphia, 1984.
19. Ramakrishnan, V., and Aruldhas, G., *J. Raman. Spectrosc.* **18**, 147 (1987).
20. Rao, K. M., Gobetto, R., Iannibello, A., and Zecchina, A., *J. Catal.* **119**, 512 (1989).
21. Eischens, R. P., Francis, S. A., and Pliskin, W. A., *J. Phys. Chem.* **60**, 194 (1956).
22. Eischens, R. P., and Pliskin, W. A., *Adv. Catal.* **10**, 1 (1958).
23. Penninger, J. M. L., *J. Catal.* **56**, 287 (1979).
24. Rebensdorf, B., and Larsson, R., *Z. Anorg. Allg. Chem.* **453**, 127 (1979).
25. Rebensdorf, B., Lindblad, T., and Andersson, S. L. T., *J. Catal.* **128**, 293 (1991).
26. Rebensdorf, B., and Lindblad, T., *J. Catal.* **128**, 303 (1991).
27. Hicks, R. F., Kellner, C. S., and Savatsky, B. J., *J. Catal.* **71**, 216 (1981).
28. Rothwell, W. P., Waugh, J. S., and Yesinowski, J. P., *J. Am. Chem. Soc.* **102**, 2637 (1980).
29. Martin, M. L., Martin, G. L., and Delpuech, J.-J., "Practical NMR Spectroscopy." Heyden, Philadelphia, 1980.
30. Emsley, J., and Hall, D., "The Chemistry of Phosphorus." Wiley, New York, 1976.
31. Gunter, G. C., "Catalytic Upgrading of Lactic Acid over Supported Salt Catalysts." Ph.D. Dissertation, Michigan State Univ., 1994.
32. Van Wazer, J. R., "Phosphorus and Its Compounds, Vol. 1: Chemistry." Interscience, New York, 1958.
33. Greenfield, S., and Clift, M., "Analytical Chemistry of the Condensed Phosphates." Pergamon, New York, 1975.
34. Haubenreisser, U., Scheler, G., and Grimmer, A.-R., *Z. Anorg. Alleg. Chem.* **532**, 157 (1986).
35. Irani, R. R., and Callis, C. F., *J. Phys. Chem.* **65**, 934 (1961).
36. Wall, F. T., and Doremus, R. H., *J. Am. Chem. Soc.* **76**, 868 (1954).
37. Wendrow, B., and Kobe, K. A., *Ind. Eng. Chem.* **44**, 1439 (1952).
38. Bell, R. N., *Ind. Eng. Chem.* **41**, 2901 (1949).
39. Schroeder, W. C., Berk, A. A., and Gabriel, A., *Ind. Eng. Chem.* **59**, 1783 (1937).
40. Wendrow, B., and Kobe, K. A., *Chem. Rev.* **54**, 891 (1954).